Title:

DNA-PK controls cyclic dinucleotide-associated type I Interferon responses

Authors :

Clara Taffoni[1], Isabelle K. Vila[1], Jane Jardine[2], Moritz Schussler[1], Joe McKellar[1], Morgane Chemarin[1], Joanna Re[1], Yasmine Messaout-Nacer[1], Insaf El Mansouri[1], George P Chrousos[3], Nicolas Bidère[2], Karim Majzoub[1], Dimitrios Vlachakis[3,4,5,*], Nadine Laguette[1,*]

Affiliations :

[1] IGMM, université de Montpellier, CNRS UMR5535, Montpellier, France

[2] Team SOAP, CRCI2NA, Nantes Université, Inserm, CNRS, Université d'Angers Nantes France, Equipe Labellisée Ligue Contre le Cancer Paris France

[3] Laboratory of Genetics, Department of Biotechnology, School of Applied Biology and Biotechnology, Agricultural University of Athens, 75 Iera Odos, 11855 Athens, Greece

[4] University Research Institute of Maternal and Child Health & Precision Medicine, and UNESCO Chair on Adolescent Health Care, National and Kapodistrian University of Athens, "Aghia Sophia" Children's Hospital, 11527 Athens, Greece

[5] School of Informatics, Faculty of Natural & Mathematical Sciences, King's College London, WC2R 2LS, Bush House, Strand, London, U.K.

*Correspondance to :

Nadine Laguette : nadine.laguette@cnrs.fr; nadine.laguette@igmm.cnrs.fr; and Dimitrios Vlachakis : dimitris@aua.gr

Summary (200words):

Cytosolic dsDNAs are potent immune-stimulatory molecules that trigger inflammation in several human pathologies [1,2]. A major pathway for the detection of cytosolic dsDNA relies on the cyclic GMP-AMP (cGAMP) synthase (cGAS) that produces the 2'3'-cGAMP cyclic dinucleotide (CDN) for activation of the Stimulator of Interferon Genes (STING) adaptor protein that subsequently drives type I Interferon (IFN) responses [3,4]. Here, we investigated the mechanism regulating intracellular 2'3'-cGAMP levels. We show that the DNA-dependent protein kinase catalytic subunit (DNA-PKcs), a major player in the repair of double-strand breaks, directly regulates intracellular levels of 2'3'-cGAMP, thereby reducing STING activation. We describe that the binding of 2'3'-cGAMP to DNA-PKcs occurs in its catalytic cleft, impeding its kinase function. Contrary to other CDN regulatory mechanisms that have been shown to primarily regulate extracellular 2'3'-cGAMP, we show that DNA-PKcs also interacts with the 3'3'-cGAMP bacterial CDN, limiting its capacity to activate STING signaling. Furthermore, we found that DNA-PKcs decreases the potency of pharmacological STING activators. As STING is a major target for therapeutic interventions aiming to boost inflammatory responses in immunosuppressed contexts [5], our data bear important implications for drug development and deepens our understanding of inflammatory regulation in response to CDNs.

Main text:

The presence of DNA in the cytosol is sensed as a danger signal and promotes the activation of inflammatory responses [6]. A major pathway involved in the detection of cytosolic dsDNA relies on the cyclic GMP-AMP (cGAMP) synthase (cGAS) [7] that catalyzes the production of the 2'3'-cGAMP cyclic dinucleotide (CDN), which in turn binds and activates the Stimulator of Interferon Genes (STING) adaptor protein [8]. The interaction of 2'3'-cGAMP with STING drives the assembly of a signalosome where the Tank Binding Kinase 1 (TBK1) catalyzes phosphorylation-dependent activation of transcription factors, such as the Interferon Regulatory Factor 3 (IRF3), that drive the expression of inflammatory cytokines and type I Interferons (IFNs) [9,10]. Activation of the cGAS-cGAMP-STING signaling axis is essential in response to pathogen infection, cellular stress, or tissue damage which are contexts where immune stimulatory dsDNAs are exposed in the cytosol. However, chronic activation of this signaling pathway is reported in several human pathologies, such as auto-inflammatory diseases or

53 cancer, where it is responsible for chronic low-grade disease-promoting inflammation, leading
54 to immune dysfunction and tissue damage [6].

55 To mitigate the deleterious effects of unwanted activation of the cGAS-cGAMP-STING
56 pathway, several regulatory layers have been described to control directly cGAS and/or STING
57 activation [11,12]. In contrast, few direct regulators of the 2'3'-cGAMP molecule have been
58 documented in mammals [13-15], all of which expected to act on extracellular 2'3'-cGAMP. This
59 is striking since 2'3'-cGAMP is an essential component of the cGAS-STING axis involved
60 notably in signal amplification and propagation [16]. Additionally, despite several CDNs of
61 bacterial origins shown to be active in mammalian cells [17,18], no mechanism ensuring their
62 regulation has been described to date. Here, we unveil the DNA-PK catalytic subunit (DNA-
63 PKcs) of the DNA-PK complex, canonically involved in double-strand break repair, as an
64 intracellular regulator of CDNs.

65 ***DNA-PK regulates 2'3-cGAMP-associated STING signaling***

66 DNA-PK has been shown to play dichotomous roles in the regulation of STING-dependent
67 inflammatory responses. Specifically, DNA-PK can operate as an alternative cytosolic dsDNA
68 detection pathway capable of driving IFN signaling [19,20] and as a co-activation of cGAS [21,22],
69 while also bearing the ability to counteract cGAS-STING activation [23]. This suggests that DNA-
70 PK regulates cGAS-STING pathway activation at several levels. Here, we tested whether DNA-
71 PK regulates inflammatory responses downstream of cGAS.

72 To this aim, we used T98G glioblastoma cells that do not express detectable cGAS levels [22].
73 T98G cells were treated with the 2'3'-cGAMP CDN in the presence or absence of NU7441, a
74 selective DNA-PK inhibitor [24]. Western blot (WB) analyses showed the expected STING-
75 dependent signaling activation in the presence of 2'3'-cGAMP, as demonstrated by STING
76 degradation, as well as phosphorylation of STING and IRF3 (Fig. 1a). Analyses of the
77 expression of transcripts associated with STING activity, such as *IFNB1*, *ISG15*, *IFIT1*, and
78 *CCL5* also showed the expected increase in response to 2'3'-cGAMP-mediated stimulation
79 (Fig. 1b). Interestingly, treatment with 2'3'-cGAMP in combination with NU7441 led to
80 increased pSTING and pIRF3 levels (Fig. 1a) and enhanced the expression of *IFNB1*, *ISG15*,
81 *IFIT1*, and *CCL5*, as compared to treatment with 2'3'-cGAMP alone (Fig. 1b). To assess
82 whether 2'3'-cGAMP in combination with NU7441 led to a biologically-relevant enhancement
83 of type I IFN responses, we tested its impact on infection with the herpes simplex virus 1 (HSV-

84 1) DNA virus known to be sensitive to type I IFN responses [25]. We treated T98G cells with
85 2'3'-cGAMP and NU7441 individually or in combination prior to infection with a green
86 fluorescence protein (GFP)-encoding HSV-1 molecular clone (HSV-1-GFP) and assessed the
87 percentage of GFP-positive cells. We found that NU7441 boosted the inhibitory impact of 2'3'-
88 cGAMP on HSV-1-GFP infection compared to treatment with 2'3'-cGAMP alone, attesting to
89 an enhancement of the antiviral status of cells by the combination of 2'3'-cGAMP and NU7441
90 (Fig. 1c). These results indicate that inhibition of DNA-PK leads to enhanced 2'3'-cGAMP-
91 associated signaling and antiviral activity, suggesting that DNA-PK may inhibit 2'3'-cGAMP
92 signaling in T98G cells.

93 DNA-PK is a holoenzyme comprised of three subunits. KU70 and KU80 form heterodimers
94 that ensure the recruitment of the DNA-PK catalytic subunit (DNA-PKcs) to nuclear double-
95 strand breaks to ensure repair by non-homologous end-joining [26], but also to cytosolic dsDNA
96 to participate to type I IFN signaling [22]. Because NU7441 specifically inhibits the DNA-PKcs
97 subunit of DNA-PK, our data suggest that DNA-PKcs may be sufficient to mediate the
98 inhibition of 2'3'-cGAMP-associated signaling. We thus next used small interfering RNAs
99 (siRNAs) targeting DNA-PKcs or the KU70 subunits of DNA-PK (Extended data Fig. 1a-b)
100 and assessed the impact on 2'3'-cGAMP-dependent STING activation. Treatment with 2'3'-
101 cGAMP following knock-down of DNA-PKcs, but not of KU70, led to increased expression of
102 STING-associated transcripts such as *IFNB1*, *ISG15*, *IFIT2* and *CCL5* (Extended data Fig. 1c),
103 phenocopying the effect of treatment with NU7441. Hence, our data supports that the absence
104 of DNA-PKcs is sufficient to enhance 2'3'-cGAMP-associated type I IFN responses.

105 ***DNA-PKcs-dependent control of inflammatory responses operates upstream of STING***

106 We next asked at which level the DNA-PKcs-mediated inhibition of 2'3'-cGAMP signaling
107 operates. The fact that this phenotype can be observed in T98G cells that lack cGAS expression
108 [22] suggests that DNA-PKcs operates downstream of cGAS but upstream of STING.

109 To confirm this observation, we next used THP-1 myeloid cells that are cGAS and STING
110 proficient, as well as THP-1 cells knock-out for cGAS (THP-1$^{cGAS-/-}$) or STING (THP-1$^{STING-/-}$
111). Control THP1 cells (THP-1^{CTRL}), THP-1$^{cGAS-/-}$ and THP-1$^{STING-/-}$ were mock treated or treated
112 with 2'3'-cGAMP and NU7441 individually or in combination. Gene expression and WB
113 analyses showed that combining 2'3'-cGAMP treatment with DNA-PK inhibition boosted the
114 activation of STING-dependent signaling in THP-1^{CTRL} but also in THP-1$^{cGAS-/-}$, resulting in

115 increased expression of *IFNB1*, *ISG15*, *CXCL10*, and *IFIT2* (Fig. 1d) and increased
116 phosphorylation of IRF3 and STING (Fig. 1e, lanes 1-4 and 5-8). In STING-deficient THP-1
117 cells, the 2'3'-cGAMP-associated response was abrogated, regardless of NU7441 treatment
118 (Fig. 1d and e, lanes 9-12). Similar results were obtained in T98G cells engineered to be
119 knocked-out for STING (T98G$^{STING-/-}$) where the absence of STING disrupted the impact of
120 2'3'-cGAMP treatment alone or in combination with DNA-PK inhibition, as attested by the
121 absence of *IFNB1*, *ISG15*, *IFIT1*, *CCL5*, and *IFIT2* expression (Extended data Fig. 1d) and
122 absence of phosphorylation of IRF3 and STING (Extended data Fig. 1e). These data support
123 that DNA-PKcs-mediated inhibition of 2'3'-cGAMP signaling is independent of cGAS but
124 requires the presence of STING.

125 We next assessed whether DNA-PKcs-associated regulation of cGAMP-dependent type I IFN
126 responses may result from STING activation and subsequent type I IFN responses though
127 stimulation of the Interferon-α/β receptor (IFNAR). To this aim, T98G cells were engineered
128 to be knock-out for IRF3 (T98G$^{IRF3-/-}$) or IFNAR (T98G$^{IFNAR-/-}$). Those cell lines as well as
129 control T98G cells (T98G^{CTRL}) were mock-treated or treated with 2'3'-cGAMP and NU7441,
130 individually or in combination. As expected, IRF3 knock-out did not alter STING
131 phosphorylation in response to 2'3'-cGAMP transfection (Extended data Fig. 1f). Importantly,
132 we found that the potentiation of STING phosphorylation when 2'3'-cGAMP and NU7441
133 treatments were combined was not altered in absence of IRF3 (Extended data Fig. 1f). Similar
134 experiments were conducted in T98G$^{IFNAR-/-}$ cells, showing that absence of IFNAR did not
135 prevent increased IRF3 and STING phosphorylation when T98G cells are treated with 2'3'-
136 cGAMP in combination with NU7441 (Extended data Fig. 1g).

137 These data demonstrate that DNA-PKcs-dependent regulation of 2'3'-cGAMP-mediated
138 inflammatory responses requires STING and is not a consequence of STING-dependent type I
139 IFN responses and therefore operates upstream of STING activation.

140 ***DNA-PKcs interacts with 2'3'-cGAMP***

141 Since DNA-PKcs exerts its inhibitory effect downstream of cGAS and upstream of STING, we
142 hypothesized that DNA-PKcs may directly regulate 2'3'-cGAMP levels and therefore decrease
143 STING activation. To test this hypothesis, we next used human embryonic kidney HEK293T
144 cells to generate control (293T^{CTRL}) and DNA-PKcs knock-out (293T$^{DNA-PKcs-/-}$) cell lines.
145 Indeed, HEK293T cells express low levels of cGAS and STING and therefore do not mount

146 measurable type I IFN responses when DNA repair is impeded by DNA-PKcs knock-out
147 (Extended data Fig. 2a). 293T^{CTRL} and 293T$^{DNA\text{-}PKcs\text{-}/\text{-}}$ were treated with 2'3'-cGAMP prior to
148 assessment of intracellular 2'3'-cGAMP levels by enzyme-linked immunosorbent assay
149 (ELISA). We found that the absence of DNA-PK resulted in increased 2'3'-cGAMP levels (Fig.
150 2a). Similarly, in T98G cells were treated with 2'3'-cGAMP in the presence or absence of
151 NU7441, we found that in T98G cells, treatment withNU7441 increased intracellular 2'3'-
152 cGAMP levels (Extended data Fig. 2b). These data suggest that increased STING activation
153 following DNA-PKcs inhibition may result from increased availability of 2'3'-cGAMP.

154 We next hypothesized that DNA-PKcs may regulate 2'3'-cGAMP levels through physical
155 interaction. We thus tested the capacity of 2'3'-cGAMP to interact with DNA-PKcs. To this
156 aim, we first immunoprecipitated DNA-PKcs from T98G cells using a DNA-PKcs-specific
157 antibody or control IgG (Extended data Fig. 2c). Immunoprecipitates were incubated with 2'3'-
158 cGAMP prior to release using proteinase K and measurement of 2'3'-cGAMP. We found that
159 the DNA-PK immunoprecipitation presented a significant enrichment in bound 2'3'-cGAMP,
160 as compared to control (Fig. 2b). Similar results were obtained when FLAG-
161 immunoprecipitating a FLAG-tagged DNA-PKcs over-expressed in HEK293T cells (Extended
162 data Fig. 2d-e). Of note, consistent with our observation that KU heterodimers are not necessary
163 for the DNA-PKcs-mediated inhibition of 2'3'-cGAMP signaling, no KU80 was detected in the
164 DNA-PKcs immunoprecipitation (Extended data Fig. 2e). To exclude further the participation
165 of DNA-PKcs co-factors in the binding to 2'3'-cGAMP, we next performed similar
166 experiments using recombinant DNA-PKcs, which was bead-immobilized using a DNA-PKcs-
167 specific antibody (Extended data Fig. 2f) prior to incubation with 2'3'-cGAMP, release and
168 measurement of recovered 2'3'-cGAMP. We found a significant enrichment of 2'3'-cGAMP,
169 when DNA-PKcs was present in the reaction (Fig. 2c), confirming that DNA-PKcs can interact
170 with 2'3'-cGAMP. Of note, when similar experiments were conducted using the 2'5'-GpAp
171 linear dinucleotide analog of 2'3'-cGAMP (thereafter, linear-cGAMP) that does not activate
172 STING (Invivogen), we did not retrieve detectable amounts of linear cGAMP in the DNA-PKcs
173 immunoprecipitates (Extended Fig. 2g-h).

174 We next aimed to identify the domain of DNA-PKcs engaged in interaction with 2'3'-cGAMP.
175 Owing to the size of DNA-PKcs we first performed *in silico* molecular modelling and docking
176 analyses to identify putative binding regions. We used the resolved crystal of human DNA-
177 PKcs (PDB: 5LUQ) as a starting biological system for docking analyses using 2'3'-cGAMP.
178 This predicted that 2'3'-cGAMP can dock into DNA-PKcs catalytic pocket (Fig. 2d and

179 Extended data Fig. 3a-b), adopting a stable conformation (Energy -28911.06 Kcal/mol, Table
180 I) notably through strong H-bonds between residues Asp3723, Arg3741, His1069 and Asp3744,
181 Arg3746, His3748 with the phosphodiester bonds within the 2'3'-cGAMP molecule (Extended
182 data Fig. 3c). Congruent with our binding assays, *in silico* molecular modeling experiments
183 performed with linear-cGAMP showed that the increased flexibility of linear-cGAMP as
184 compared to 2'3'-cGAMP rendered this molecule unstable in the catalytic site of DNA-PKcs
185 (Extended data Fig. 3d-e). The specificity of the performed *in silico* analyses was controlled
186 using other DNA-repair-related enzymes belonging to the phosphatidylinositide 3-kinase
187 (PI3K)-related kinase family, to which DNA-PK belongs, namely Ataxia Telangiectasia
188 Mutated (ATM) and Ataxia Telangiectasia and Rad3-related protein (ATR), and thus possess
189 analogous catalytic sites competent for ATP hydrolysis. The structures of ATM and ATR were
190 modelled prior to the superposition of the catalytic sites with that of DNA-PKcs and
191 comparative analysis of their catalytic cleft, predicting that 2'3'-cGAMP is unlikely to interact
192 with these catalytic domains (Extended data Fig. 4a-b). Altogether, these *in silico* data confirm
193 that 2'3'-cGAMP can bind selectively to DNA-PKcs and suggest that this interaction is likely
194 to occur in the catalytic pocket of DNA-PKcs.

195 To verify the prediction that 2'3'-cGAMP interacts with DNA-PKcs catalytic pocket, two
196 approaches were used. First, we assessed whether 2'3'-cGAMP alters DNA-PKcs catalytic
197 activity *in vitro*. We found that 2'3'-cGAMP inhibits the ability of DNA-PKcs to hydrolyze
198 ATP in a dose-dependent manner (Fig. 2e), suggesting that 2'3'-cGAMP can prevent the
199 association of DNA-PKcs with its ATP substrate. To further confirm this association, we next
200 used recombinant DNA-PKcs in immunoprecipitation assays, in which NU7441 was used as a
201 competitor. We found that NU7441 was capable of displacing the interaction of 2'3'-cGAMP
202 with DNA-PKcs (Fig. 2f), supporting that the interaction of 2'3'-cGAMP with DNA-PKcs
203 occurs in its catalytic cleft.

204 Altogether, our data show that 2'3'-cGAMP interacts with the catalytic cleft of DNA-PKcs and
205 suggest that this interaction may reduce the bioavailability of 2'3'-cGAMP for STING
206 activation.

207 ***DNA-PKcs regulates the activity of 3'3'-cGAMP***

208 To date, mammalian regulators of 2'3'-cGAMP have been shown to operate selectively [13-15].
209 We questioned the spectrum of DNA-PKcs activity on CDNs of bacterial origin. To account

210 for potential activation bias incurred by the treatment of cells with bacterial CDNs, we first
211 assessed the impact of three distinct bacterial CDNs on DNA-PKcs catalytic activity *in vitro*.
212 We used 3'3'-cGAMP [27], bis-(3'-5')-cyclic dimeric adenosine monophosphate (c-di-AMP) and
213 bis-(3'-5')-cyclic dimeric guanosine monophosphate (c-di-GMP) [28,29], all of which reportedly
214 are able to induce STING-dependent signaling. We found that, similar to what was observed
215 for 2'3'-cGAMP, 3'3'-cGAMP, but not c-di-AMP nor c-di-GMP, inhibited DNA-PKcs
216 catalytic activity in a dose-dependent manner (Fig. 3a and Extended data Fig. 5a). We next
217 assessed the binding of 3'3'-cGAMP and c-di-AMP to recombinant DNA-PKcs. We found that
218 DNA-PKcs was able to interact with 3'3'-cGAMP but not with c-di-AMP (Fig. 3b). *In silico*
219 docking analyses confirmed that 3'3'-cGAMP, but not c-di-AMP nor c-di-GMP, can interact
220 with DNA-PKcs in its catalytic cleft adopting a stable conformation (Energy -30182.10
221 Kcal/mol, Table I). Congruent with the apparent higher potency of 3'3'-cGAMP at inhibiting
222 DNA-PKcs, as compared to 2'3'-cGAMP (compare Fig. 2e and Fig. 3a), energies predicted for
223 the interaction *in silico* were slightly higher for the 3'3'-cGAMP:DNA-PKcs complex as
224 compared to the 2'3'-cGAMP:DNA-PKcs complex (Table I).

225 To further test the functional interaction between DNA-PKcs and 3'3'-cGAMP, we next treated
226 T98G and THP-1 cells with 3'3'-cGAMP alone or in combination with NU7441. We found that
227 combining 3'3'-cGAMP-treatment with DNA-PKcs inhibition enhanced STING
228 phosphorylation (Fig. 3c and Extended data Fig. 5b) in both T98G and THP-1 cells and led to
229 increased expression of STING activity-associated transcripts, namely *IFNB1*, *IFIT1*, *ISG15*,
230 and *CCL5* in T98G (Fig. 3d) and THP-1 cells (Extended data Fig. 5c), as compared to cells
231 treated only with 3'3'-cGAMP. Combined, our data show that DNA-PKcs selectively interacts
232 with 3'3'-cGAMP and inhibits its capacity to activate STING-dependent signaling, but does
233 not appear to interfere with other tested bacterial CDNs.

234 ***DNA-PKcs inhibits the activity of STING targeting drugs***

235 STING is an important biomedical target for which a plethora of agonists are tested in ongoing
236 clinical trials {Hines, 2023 #40}. Because several of these compounds have been designed
237 based on the structure of CDNs capable of activating STING, we tested whether DNA-PKcs
238 affects their potency. To this aim, T98G cells were treated with STING agonists individually
239 or in combination with NU7441. The tested STING agonists were: ADU-S100,diABZI, and
240 E7766.

241 We first investigated the impact of DNA-PK on diABZI and E7766 which are STING agonists
242 designed based on the structure of 2'3'-cGAMP. WB analyses showed that treatment with
243 E7766 or diABZI in combination with NU7441 led to enhanced IRF3 and STING
244 phosphorylation (Fig. 4a and extended data Fig. 6a) and increased expression of *IFNB1*, *ISG15*,
245 *IFIT1* and *CCL5,* compared to STING agonists alone (Fig. 4b and extended data Fig. 6b). In
246 order to assess whether the increased potency of E7766 upon DNA-PKcs inhibition results from
247 its interaction with DNA-PKcs, we measured DNA-PKcs-mediated ATP hydrolysis activity in
248 the presence of increasing doses of E7766 *in vitro*. We found that E7766 potently inhibited
249 DNA-PKcs activity (Fig. 4c), supporting a similar mechanism of action than that measured for
250 2'3'-cGAMP and 3'3'-cGAMP (Fig. 2-3).

251 Next, we assessed the impact of DNA-PKcs on ADU-S100, a compound that was designed
252 based on ci-d-AMP. In contrast to data obtained with E7766 or diABZI, treatment with ADU-
253 S100 in combination with NU7441 lead to non-significant enhancement of ADU-S100-induced
254 STING activation as shown by WB (Fig. 4d) or gene expression analysis (Fig. 4e). Furthermore,
255 *in vitro* DNA-PKcs ATP hydrolysis assays also showed that ADU-S100 fails to inhibit DNA-
256 PKcs catalytic activity (Fig. 4f). These data thus show that DNA-PKcs inhibition selectively
257 alters the efficiency of STING agonists.

258 Finally, we sought to assess whether DNA-PKcs-mediated inhibition of these compounds could
259 influence the establishment of physiologically relevant STING-associated biological responses,
260 namely antiviral responses. To this aim, we treated T98G cells with STING agonists
261 individually or in combination with NU7441, followed by infection with either HSV-1-GFP or
262 a GFP reporter expressing vesicular stomatitis virus (VSV-GFP). The latter is a RNA virus
263 known to be sensitive to type I IFN responses [30]. In agreement with previous reports [25],
264 treatment with STING agonists decreased infection by both VSV-GFP and HSV-1-GFP (Fig.
265 4g-h and Extended data Fig. 6c-d). Combining such treatments with NU7441-mediated DNA-
266 PKcs inhibition led to a more profound decrease of the percentage of VSV-GFP and HSV-1-
267 GFP infected cells (Fig. 4g-h and Extended data Fig. 6c-d). Our data therefore support that
268 DNA-PKcs can inhibit the capacity of STING agonists to induce a STING-dependent antiviral
269 responses.

270 ***Discussion***

271 In this study, we show that DNA-PKcs controls 2'3'-cGAMP and 3'3'-cGAMP CDNs-
272 associated inflammatory response. Our data supports a model in which DNA-PKcs operates by
273 binding to those CDNs selectively, decreasing their availability for interaction with STING and
274 thereby buffering their STING-associated activity. This finding is in contrast with other
275 mechanisms described to control CDN activity that appear to have specifically evolved to
276 control extracellular 2'3'-cGAMP levels [13-15], which is the only CDN described to date to be
277 produced by mammalian cells [7]. The fact that DNA-PKcs can counteract the impact of 3'3'-
278 cGAMP on immunity seems to be a distinctive feature and may have evolved as a mechanism
279 of tolerance towards 3'3'-cGAMP-producing bacteria. Phylogenetic analyses have shown that
280 DNA-PKcs is highly conserved [31], suggesting that this mechanism of action may be present
281 across the tree of life and may operate as a general mechanism to prevent overactivation of
282 inflammatory responses.

283 We and others have reported that DNA-PK can operate as a co-activator of cGAS-STING in
284 the presence of cytosolic dsDNA [19,21,22] while others reported an inhibitory role of DNA-PK on
285 antiviral responses [23]. The present study supports that DNA-PK has a dual role in modulating
286 cGAS-STING signaling, which could alter the amplitude and kinetics of dsDNA responses, as
287 well as homeostatic inflammation.

288 Importantly, we also demonstrate that 2'3'-cGAMP and 3'3'-cGAMP can block DNA-PKcs
289 catalytic activity, which may have an impact on its ability to repair double-strand breaks.
290 However, previous studies have shown that of the levels of DNA-PK do not correlate with DNA
291 repair functions [32]and that other pathways can take over NHEJ-mediated repair when DNA-
292 PKcs is non-functional [33]. While the impact of CDNs on DNA-PK-specific repair functions,
293 such as its role in micronuclei damage [34], remain to be dissected, our findings also support that,
294 as previously speculated [35,36], the role of DNA-PKcs may not be confined to DNA repair.
295 Indeed, several reports point towards multifunctional roles of DNA-PK, highlighting in
296 particular its multi-level involvement in the regulation of inflammatory responses [36].

297 Importantly, our study also shows that the ability of DNA-PKcs to control CDN-associated
298 inflammatory responses is very relevant for drugs designed on CDN-based scaffolds. Because
299 such compounds are being clinically tested, it is essential to investigate their off-target effects
300 that may lead to confounding results. For instance, it is important to assess whether these
301 compounds may bear an increased ability to interact with DNA-PKcs, thereby inducing DNA
302 repair deficiency-associated side-effects. Conversely, the status of DNA-PK in target tissues

may be important to assess in order to predict the capacity of STING agonists to induce beneficial inflammation. This is particularly relevant in the context of cancer immunotherapy where STING agonists are used to boost inflammatory responses [37]. Cancer types presenting DNA-PKcs anomalies, such as copy number variations are frequent [38]. In those contexts, our data strongly suggests that the impact of STING agonists may be altered. It is therefore important to take into account the status of DNA-PKcs in cancer patients enrolled in STING-agonist-based clinical trials for better stratification.

References

Tables

Table I. ALL: complex energy; INT: interaction energy; VDW: Van der Waals. Calculated energies are expressed in kcal.mol-1

		Energy	Strain	VDW	Electrostatic
2’3’-cGAMP	ALL	-28911.06	1388.79	6972.41	-38159.41
	INT	-172.03	0.00	34.28	-206.31
3’3’-cGAMP	ALL	-30182.10	1050.79	6169.34	-38204.66
	INT	-252.10	0.00	-40.74	-21.35

316 **Figures and Legends**

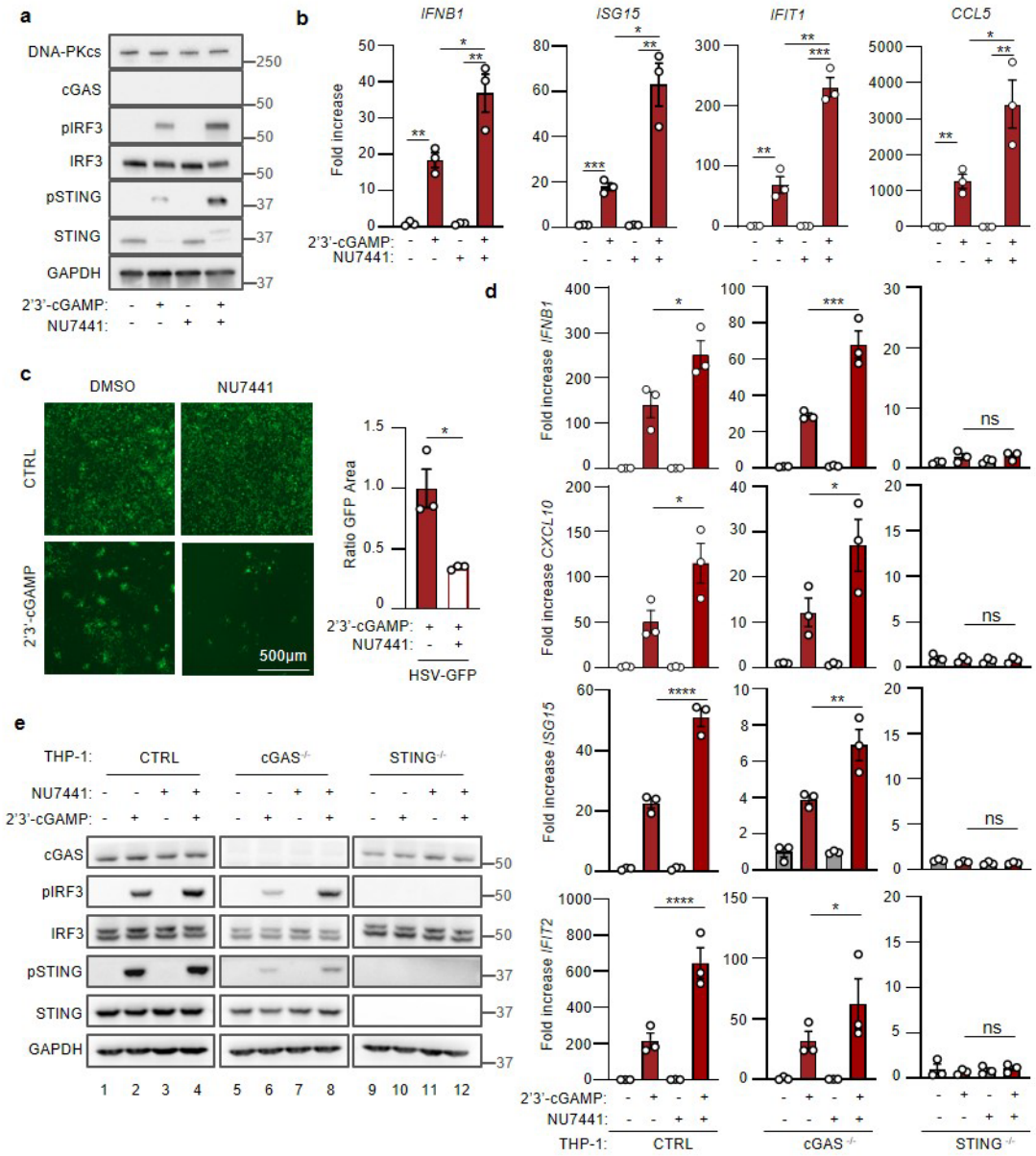

317

318 **Figure 1. DNA-PK inhibits 2'3'-cGAMP signaling. a,** T98G cells were treated or not with
319 2µM the NU7441 DNA-PKcs inhibitor for 1 hour prior to transfection or not of 10µg/ml 2'3'-
320 cGAMP for 6 hours and analysis of whole cell extract by Western blot (WB) using the indicated
321 antibodies. WB is representative of at least 3 independent experiments. **b**, As in **a**, except that
322 gene expression analysis was conducted. Graphs present the mean ± standard error from the
323 mean (SEM) of 3 independent experiments. **c**, T98G cells were pretreated or not for 1 hour with
324 2µM NU7441 prior to transfection of 10µg/ml 2'3'-cGAMP for 6 hours prior to infection with
325 HSV-1-GFP. Images are representative of 3 independent experiments. Graphs shows the
326 relative change of the GFP signal between the indicated conditions, following normalization to

327 their own controls in 3 independent experiments. **d,** THP-1 cells expressing a control gRNA
328 (CTRL), or cGAS- or STING-targeting gRNAs were treated or not with 2µM of the NU7441
329 DNA-PKcs inhibitor for 1 hour prior to transfection of not of 10µg/ml 2'3'-cGAMP for 6 hours
330 and gene expression analysis. Graphs present the mean (±SEM) of 3 independent experiments.
331 **e**, As in **d** except that whole cell extracts were analyzed by WB using the indicated antibodies.
332 WB are representative of 3 independent experiments. Statistical significance was calculated by
333 Student T-test. ****: p<0.0001; ***: p<0.001; **: p<0.01; *: p<0.05; ns: not significant.

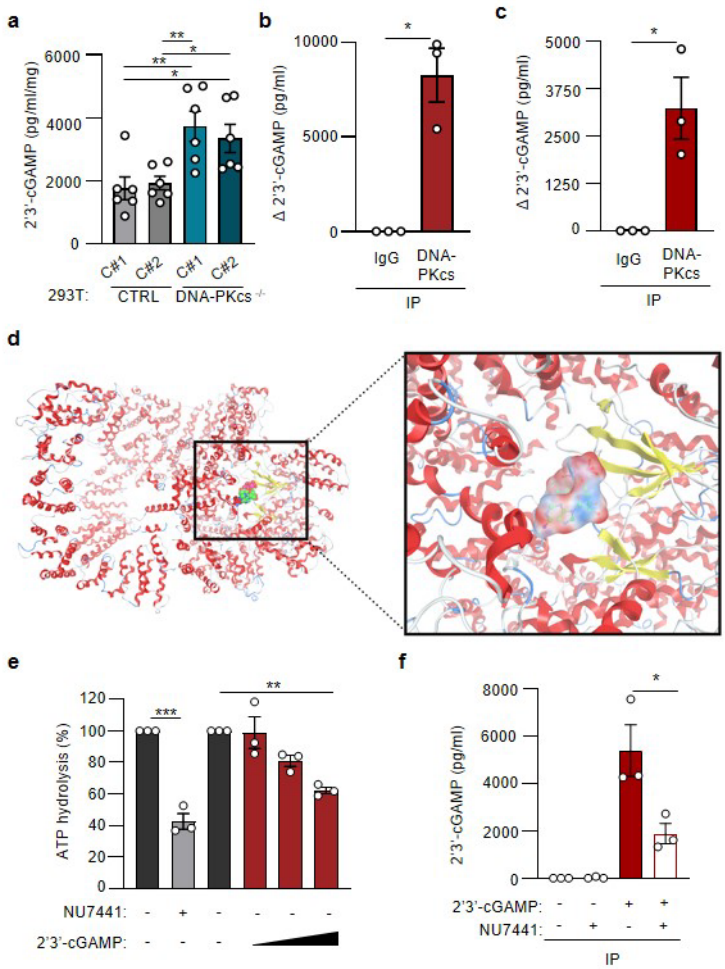

334

335 **Figure 2. 2'3'-cGAMP interacts with DNA-PKcs catalytic pocket. a.** 293T cells expressing
336 control gRNA or DNA-PKcs-targeting gRNAs were transfected with 10µg/ml 2'3'-cGAMP for
337 3 hours prior to measurement of intracellular 2'3'-cGAMP levels. The graph presents the
338 increased 2'3'-cGAMP levels as measured from 6 independent experiments. **b**, Whole cell
339 extracts from T98G cells were used to perform immunoprecipitations using either mock IgG to
340 a DNA-PKcs-specific antibody prior to incubation of immunoprecipitates with 2'3'-cGAMP
341 and measurement of bound 2'3'-cGAMP. Graph represents mean (±SEM) 2'3'-cGAMP levels

342 as measure in Mock and DNA-PK-specific IP. Graph presents the mean of 3 independent
343 experiments. **c**, As in b, except that immunoprecipitation was performed on recombinant DNA-
344 PK. Graph presents the mean (±SEM) of 3 independent experiments. **d**, Representation of the
345 molecular modeling of 2'3'-cGAMP in interaction with DNA-PKcs. **e**, ATP hydrolysis by
346 DNA-PK was measured in vitro in presence of NU7441 or increasing doses 300µM- 2700µM
347 of 2'3'-cGAMP. Graph presents the mean of 3 independent experiments. **f**, As in d, except that
348 the NU7741 inhibitor was used as a competitor. Statistical significance in a, c, d and f was
349 calculated by Student T-test. A one-way Anova was performed for the 2'3'-cGAMP ramp in
350 panel e. ***: p<0.001; **: p<0.01; *: p<0.05.

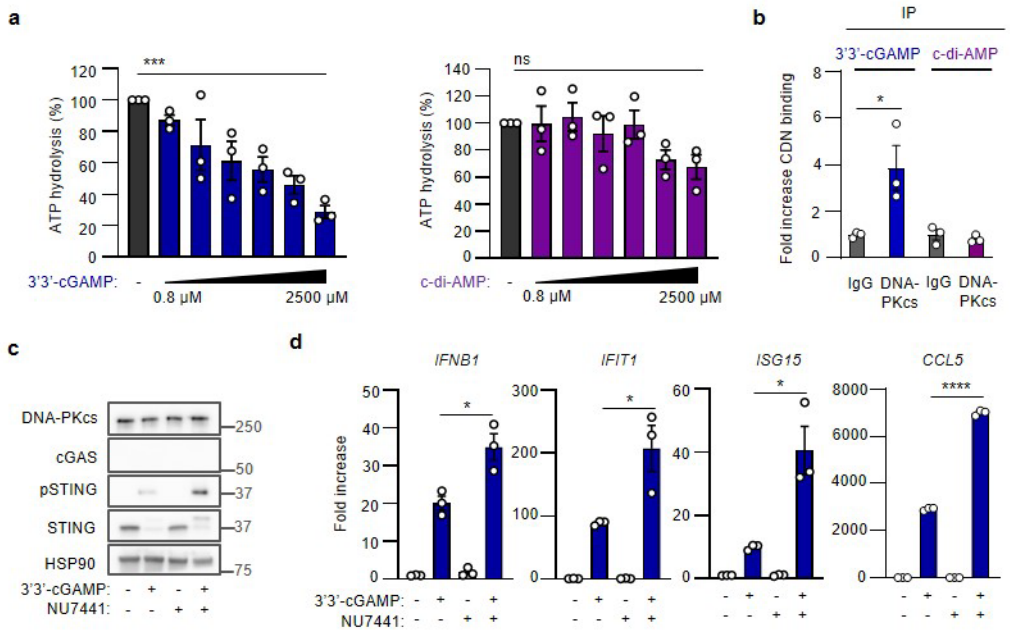

351

352 **Figure 3. DNA-PKcs inhibits 3'3'-cGAMP-associated STING activation. a**, ATP hydrolysis
353 by DNA-PK was measured in vitro in presence of increasing doses (0.8 µM to 2500 µM) of
354 3'3'-cGAMP or c-di-AMP. Graph presents the mean of 3 independent experiments. Statistical
355 significance was calculated by ANOVA. ***: p<0.001; ns: not significant. **b**, Recombinant
356 DNA-PKcs was immunoprecipitated using either mock IgG to a DNA-PKcs-specific antibody
357 prior to incubation with 3'3'-cGAMP or c-di-AMP and ELISA-based measurement of bound
358 CDNs. Graph represents mean (±SEM) 2'3'-cGAMP levels as measure in Mock and DNA-
359 PKcs-specific IP in 3 independent experiments. **c.** T98G cells were treated or not with 2µM
360 NU7441 prior to addition or not of 10µg/ml fluorinated 3'3'-cGAMP for 6 hours and analysis
361 of whole cell extracts by WB using indicated antibodies. WB are representative of at least 3
362 independent experiments. **d**, Gene expression analyses were conducted on T98G cells treated

363 as in **c**. Graphs present the mean (±SEM) of biological triplicates, representative of 3
364 independent experiments. Statistical significance was calculated by Student T-test. ****:
365 p<0.0001; *: p<0.05.

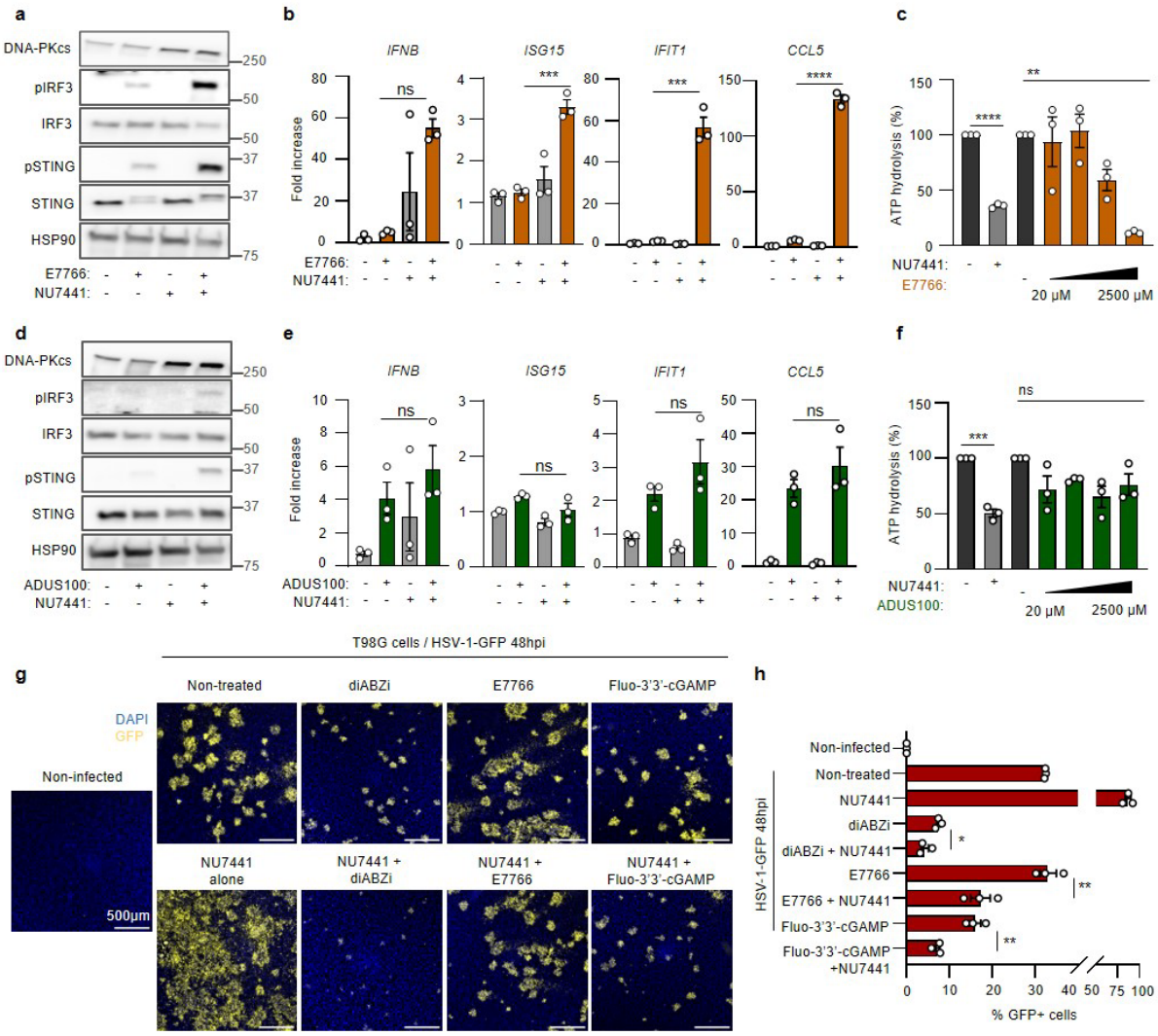

366

367 **Figure 4. DNA-PKcs inhibits the activity of STING agonists. a**, T98G cells were treated or
368 not with 2µM of NU7441 prior to addition or not of 1µM of E7766 STING agonist for 3 hours
369 and analysis of whole cell extracts by WB using indicated antibodies. WB is representative of
370 at least 3 independent experiments. **b**, gene expression analyses were conducted on T98G cells
371 treated as in **a**. Graphs present the mean (±SEM) of at least 3 independent experiments
372 performed in biological triplicates. **c**, ATP hydrolysis by DNA-PK was measured *in vitro* in
373 presence of increasing doses (0.8 µM to 2500 µM) of E7766. Graph presents the mean of 3
374 independent experiments. Statistical significance was calculated by one-way ANOVA for the
375 E7766 ramp. **d**. T98G cells were treated or not with 2µM of NU7441 prior to addition or not of
376 50µM of the ADUS100 STING agonist for 3 hours and analysis of whole cell extracts by WB

using indicated antibodies. WB is representative of at least 3 independent experiments. **e**, gene expression analyses were conducted on T98G cells treated as in **d**. Graphs present the mean (±SEM) of at least 3 independent experiments performed in biological triplicates. Statistical significance was calculated by Student T-test. ns: not significant. **f**, ATP hydrolysis by DNA-PK was measured *in vitro* in presence of increasing doses (0.8 µM to 2500 µM) of ADU-S100. Graph presents the mean of 3 independent experiments. Statistical significance was calculated by one-way ANOVA for the ADU-S100 ramp. **g**, T98G cells were treated with the diABZI, E7766 or fluorinated 3'3'-cGAMP agonists in combination of not with 2µM of NU7741. Cells were subsequently infected or not with HSV-1-GFP for 48 hours, DAPI nuclear staining and image acquisition. Images are representative of 3 independent experiments performed in biological triplicates. **h.** Graph presents the quantification of GFP signal in experiments conducted as in **g**. Statistical significance was calculated by Student T-test. Unless otherwise stated. ****: $p<0.0001$; ***: $p<0.001$; **: $p<0.01$; *: $p<0.05$; ns: not significant.

Acknowledgments: We thank all members of the Molecular Basis of Inflammation laboratory for their critical reading of this manuscript. We thank Caroline Bertin, Johanna Marines, Amel Bouzid, Mathilde Saccas for technical assistance. We thank Soren Paludan for control, STING- and cGAS-deficient THP-1 cell lines and HSV-1-GFP. We acknowledge the MRI imaging facility, member of the national infrastructure France-BioImaging infrastructure supported by the French National Research Agency (ANR-10-INBS-04, "Investments for the future").

This work was co-funded by the European Union (ERC, SENTINEL 101087092 to NL; DELV 101039538 to KM). Views and opinions expressed are however those of the author(s) only and do not necessarily reflect those of the European Union or the European Research Council. Neither the European Union nor the granting authority can be held responsible for them. This work was also co-funded by : the ANR [AlphA(NL), dezincRNA to (KM)]; l'Institut National du Cancer INCa_1884 (NB)]; LA Ligue pour la recherche contre le cancer [AAPARN 2021.LCC/JuF (NL), équipe labellisée (NB)], the Agence Nationale de Recherche sur le SIDA et les Hépatites virales (ANRS) [ECTZ117448 (NL) and fellowships to CT and JMK], the I-SITE Excellence Program of the University of Montpellier, under the Investissements France 2030 [RETTiNA (NL), ChoiCe (NL)], the Fondation ARC [ARCPJA2021060003720 COPALYS (NL), ARCPJA2021060003886 (NB)], La Région Languedoc Roussillon [Prématuration 2021 MODULON 21015964 (NL)], Fondation de France [fellowship (JJ)] and the Centre National de La Recherche Scientifique [Prématuration CNRS (NL)].

Author contributions: Conceptualization: NL, DV; Methodology: CT, NL, DV; Investigation: CT, IKV, MS, JJ; JMK, MC, IEM; Visualization: CT, DV, IKV, NL; Funding acquisition: NL, KM, NB; Project administration: NL; Supervision: NL, DV, IKV, GPC, NB, KM; Writing – original draft: NL; Writing – review & editing: NL, DV, CT, IKV, MS, JJ, JMK; KM, NB, DV.

Competing interests: Authors declare that they have no competing interests.

Materials and correspondence: Correspondence and requests for material should be addressed to Nadine Laguette and Dimitrios Vlachakis.

Extended data Figures and Legends

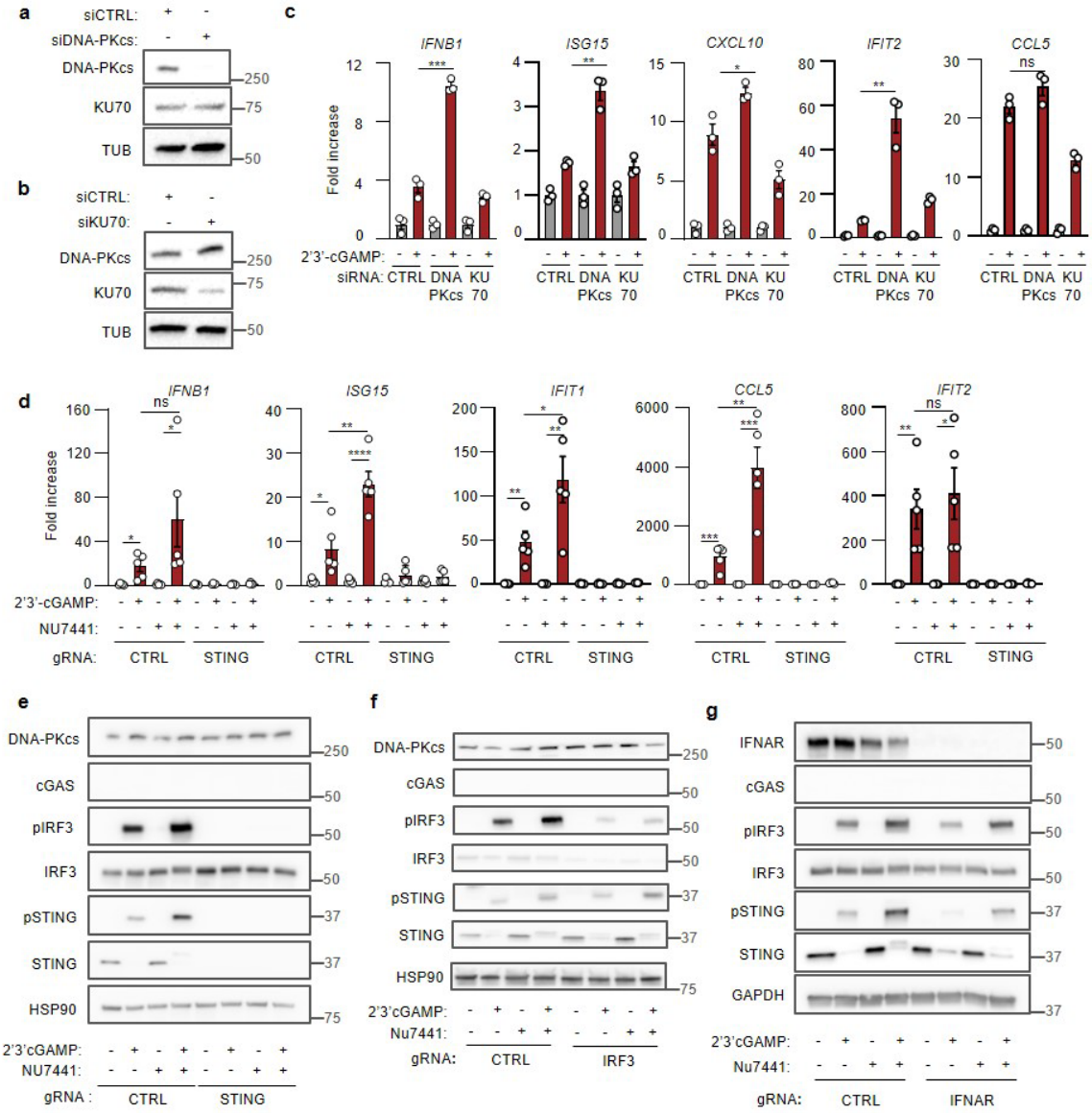

Extended data Figure 1. DNA-PK inhibits 2'3'-cGAMP signaling. a-b, T98G cells were transfected for DNA-PKcs- or KU70-targeting siRNA or a control non targeting siRNA for 48 hours prior analysis of knockdown efficiency by WB using the indicated antibodies. **c**, T98G cells were transfected for DNA-PKcs- or KU70-targeting siRNA or a control non targeting siRNA prior to transfection or not of 2'3'-cGAMP for 6 hours and gene expression analyses Graphs present the mean (±SEM) of 3 independent experiments. **d,** T98G cells engineered to express control non-targeting or STING-targeting gRNAs were treated or not with 2µM of NU7441 prior to Mock transfection or transfection of 10µg/ml 2'3'-cGAMP and gene expression analysis. **e**, as in **d** except that WB analysis was performed using the indicated antibodies. **f**, as in **e**, except that T98G cells expressing a IRF3-targeting gRNA were used. **g**,

429 as in **e**, except that T98G cells expressing an IFNAR-targeting gRNA were used. WB are
430 representative of at least 3 independent experiments. Statistical significance was calculated by
431 Student T-test. ***: p<0.001; **: p<0.01; *: p<0.05; ns: not significant.

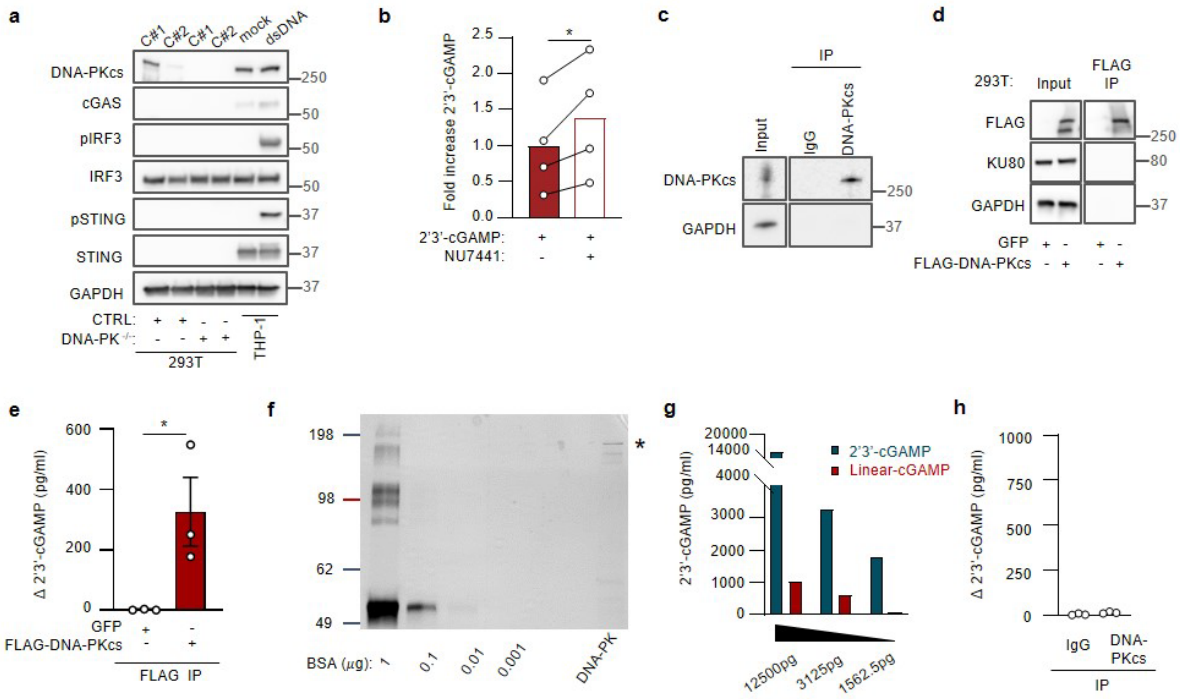

432

433 **Extended data Fig 2. 2'3'-cGAMP interacts with DNA-PKcs. a**, Whole cell extract of 293T
434 cells engineered to express a control of DNA-PKcs-targeting gRNA were analyzed by WB
435 using the indicated antibodies. C#: clone. **b**, T98G cells were treated with 2μM NU7741 for 1
436 hour prior to 2'3'-cGAMP transfection for 3 hours and analysis of intracellular 2'3'-cGAMP
437 levels. Graph presents the mean (±SEM) of 4 independent experiments. **c**, WB analysis of
438 DNA-PKcs IP used in Figure 2c was conducted using the indicated antibodies. **d**, FLAG-tagged
439 DNA-PKcs was expressed in 293T$^{DNA\text{-}PKcs\text{-}/\text{-}}$ (C#2) prior to FLAG immunoprecipitation. WB
440 analysis of Input material and FLAG IP was conducted using the indicated antibodies. **e**.
441 Immunoprecipitated material obtained as in d was incubated with 2'3'-cGAMP. Bound 2'3'-
442 cGAMP was measured by ELISA. **f**, Silver-staining was conducted on immunoprecipitated
443 recombinant DNA-PKcs used in figure 2. **g**, The detection range of linear-cGAMP as compared
444 to 2'3'-cGAMP was estimated using ELISA. **h**, Recombinant DNA-PKcs was used to perform
445 immunoprecipitations using either mock IgG to a DNA-PKcs-specific antibody prior to
446 incubation of immunoprecipitates with Linear-cGAMP and measurement of bound 2'3'-
447 cGAMP. Graph represents mean (±SEM) 2'3'-cGAMP levels as measure in Mock and DNA-

448 PKcs-specific IP. All WBs are representative of 3 independent experiments. Statistical
449 significance was calculated by Student T-test. *: p<0.05.

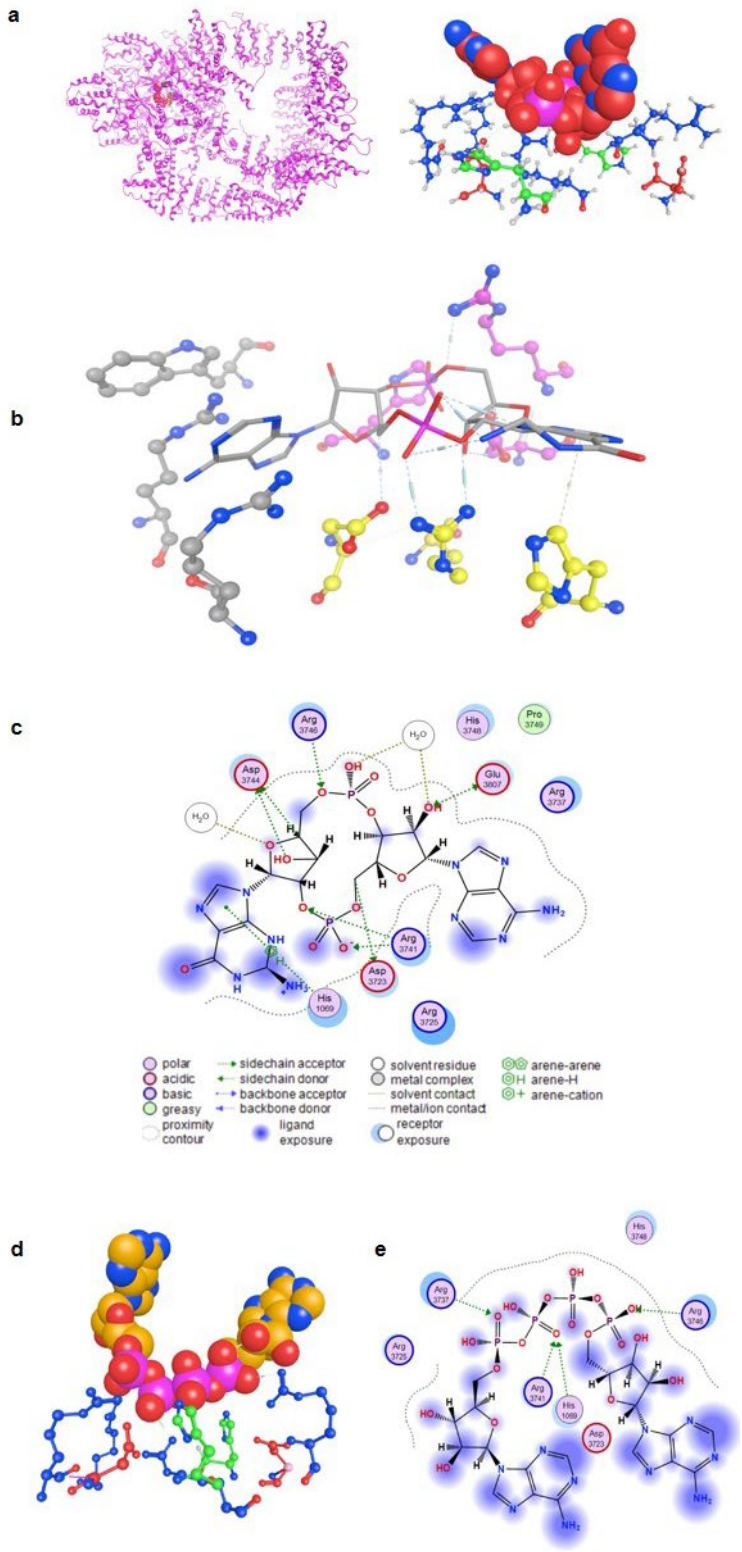

450

451 **Extended data Fig. 3. 2'3'-cGAMP but not Linear-cGAMP is predicted to interact with**
452 **the catalytic cleft of DNA-PKcs. a**, Molecular modelling and docking study of 2'3'-cGAMP

453 into DNA-PKcs. Left: Human DNA-PKcs in ribbon representation with 2'3'-cGAMP docked
454 in its catalytic site. Right: The docking conformation of 2'3'-cGAMP (in red spacefill
455 representation) into the catalytic site of DNA-PKcs in the proximity of the catalytic residues (in
456 ball and stick representation). **b**, The docked conformation adopted by 2'3'-cGAMP onto the
457 catalytic site of DNA-PKcs upon the Molecular Dynamics simulations. **c**, The 2D molecular
458 interactions diagram of 2'3'cGAMP with the catalytic residues of DNA-PKcs. **d,** Molecular
459 modelling and docking study of the Linear-cGAMP into DNA-PKcs. The docking
460 conformation of linear cGAMP (in spacefill representation) into the catalytic site of DNA-PKcs
461 in the proximity of the catalytic residues (in ball and stick representation). **e,** The 2D molecular
462 interactions diagram of Linear-cGAMP with the catalytic residues of DNA-PKcs.

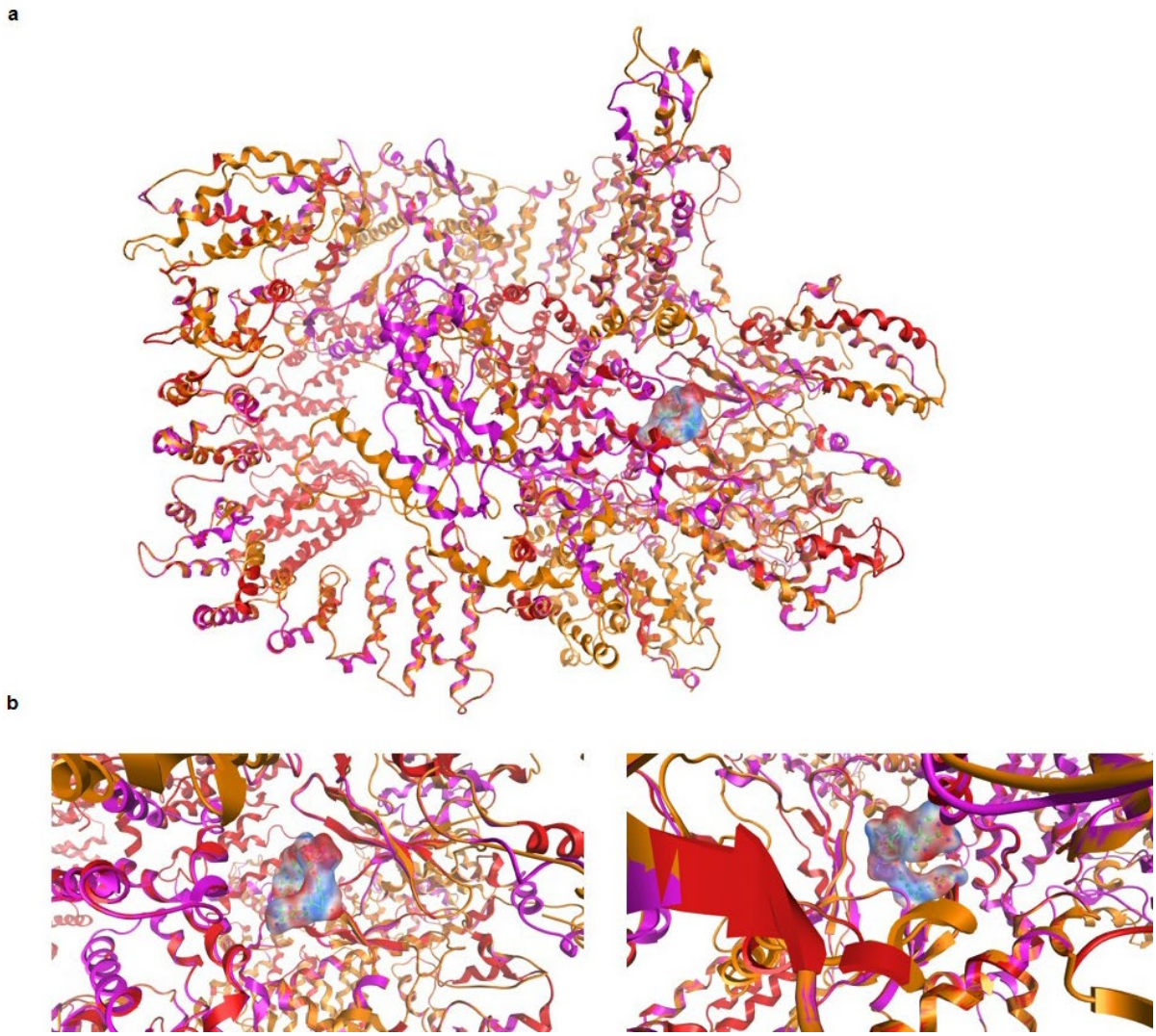

463

464 **Extended data Fig. 4. 2'3'-cGAMP is unlikely to interact with ATM or ATR. a,** Molecular
465 modelling of ATM and ATR. DNA-PKcs superposed to the models of ATM and ATR (in red,
466 magenta and orange ribbon representations respectively). **b,** Close-up of the superposed active

467 sites. Each of the 3 kinases has significant conformational differences and docking of 2'3'-
468 cGAMP to all of them failed to return a thermodynamically viable pose (complex
469 conformation).

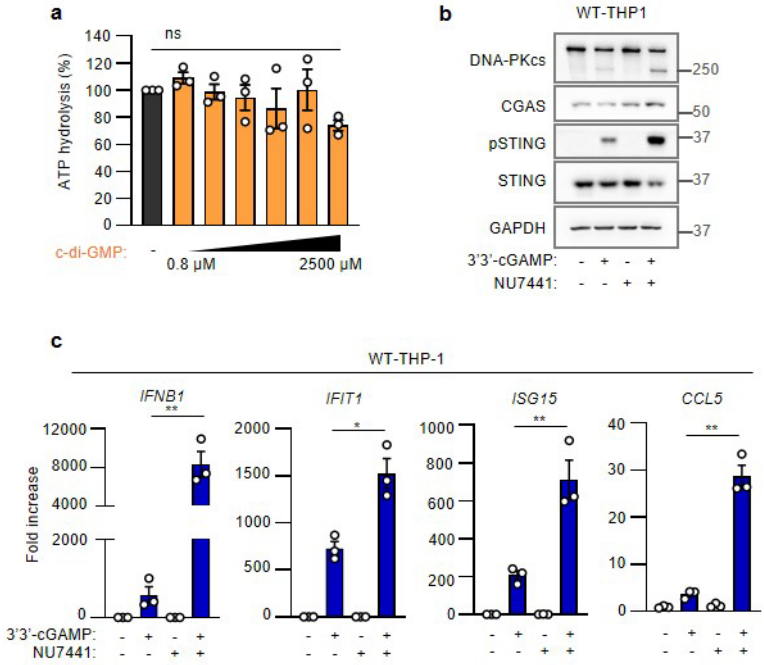

470

471 **Extended data Fig. 5. DNA-PKcs selectively counteracts CDNs. a**, ATP hydrolysis by DNA-
472 PKcs was measured in vitro in presence of increasing doses (0.8 µM to 2500 µM) of c-di-GMP.
473 Graph presents the mean (±SEM) of 3 independent experiments. Statistical significance was
474 calculated by one-way ANOVA. ns: not significant. **b**, THP-1 cells were treated or not with 2
475 µM NU7741 in combination or not with 10µg/ml fluorinated 3'3'-cGAMP for 6 hours prior to
476 WB analysis using the indicated antibodies. WB is representative of 3 independent experiments.
477 **c**, As in b, except that gene expression analyses were conducted. Graphs present the mean
478 (±SEM) of 3 independent experiments performed in biological triplicates. Statistical
479 significance was calculated by Student T-test. ***: $p<0.001$; **: $p<0.01$; *: $p<0.05$.

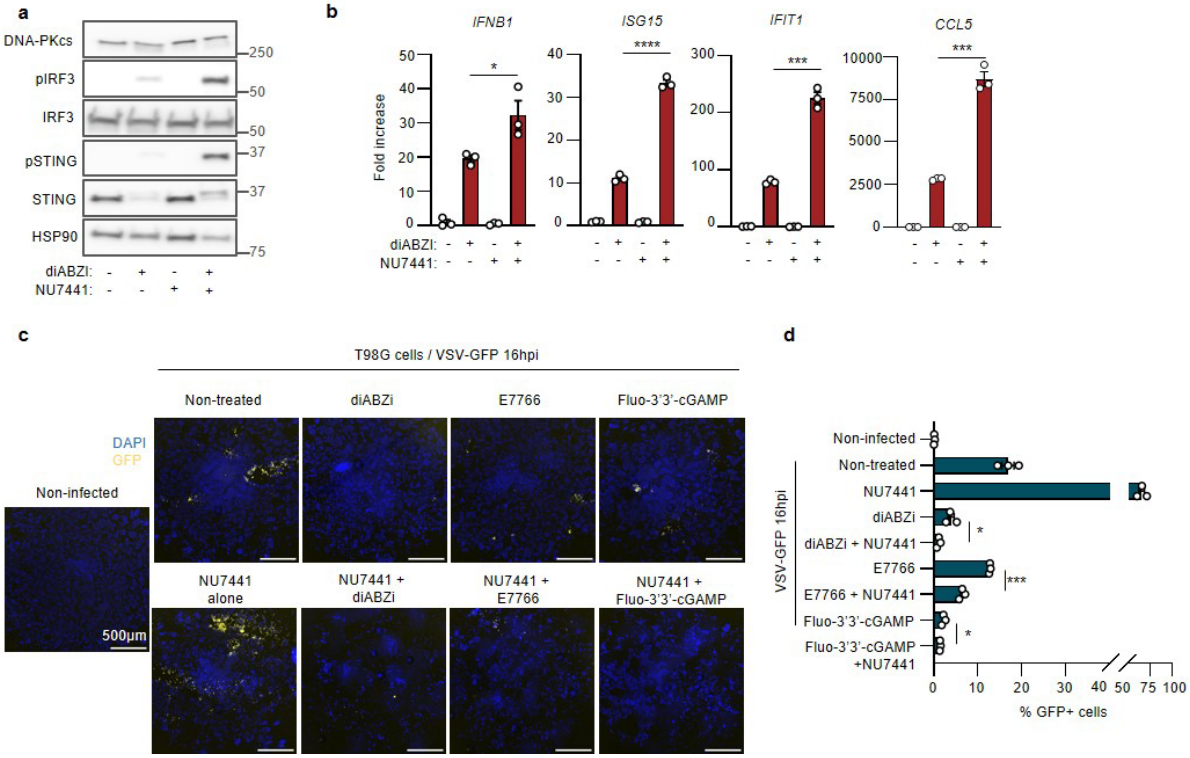

Extended Data Fig. 6. DNA-PKcs inhibits the activity of STING agonists. a, T98G cells were treated or not with 2µM NU7741 for 1 hour prior to addition or not of 10µM of diABZI for 3 hours prior to WB analysis using the indicated antibodies. WB are representative of at least 3 independent experiments. **b**, As in a, except that gene expression analyses were conducted. Graphs in c and e present the mean (±SEM) of 3 independent experiments performed in biological triplicates. Statistical significance was calculated by Student T-test. ****: $p<0.0001$; ***: $p<0.001$; **: $p<0.01$; *: $p<0.05$. **c**, T98G cells were treated with the diABZI, E7766 or 3'3'-cGAMP agonists in combination or not with 2µM of NU7441. Cells were subsequently infected or not with VSV-GFP for 16 hours, DAPI nuclear staining and image acquisition. Images are representative of 3 independent experiments performed in biological triplicates. **d**, Graphs present the quantification of GFP signal in experiments conducted as in **c**.

Methods

<u>Cells and Cell Culture:</u>

T98G cells were a gift from Caroline Goujon (IRIM, Montpellier, France). Control THP-1, cGAS-deficient THP-1 (THP-1$^{cGas-/-}$) and STING-deficient THP-1 (THP-1$^{Sting-/-}$) were a gift of S. R. Paludan (Aarhus university, Aarhus, Danemark). Vero (African green monkey),

498 HEK293T (*Homo sapiens*) and THP-1 (*Homo sapiens*) cells were obtained from the American
499 Type Culture Collection (ATCC).

500 T98G$^{STING-/-}$, T98G$^{IRF3-/-}$ and their control counterparts were previously generated using the
501 CRISPR-Cas9 technology [22]. Parental and genetically engineered T98G, HEK293T, and Vero
502 cells were maintained in Dulbecco's Modified Eagle Medium (DMEM) supplemented with 10
503 % Fetal Bovine Serum (FBS, Eurobio), 1% L-glutamine (Lonza), 1% Penicillin/Streptomycin
504 (Lonza). THP-1 cells (Cat#TIB-202, ATCC) were cultured in Roswell Park Memorial Institute
505 (RPMI, Lonza) supplemented with 20% FBS, 1% penicillin/streptomycin and 1% L-glutamine.
506 All cell lines were maintained at 37 °C, under 5% CO_2.

507 Drugs:

508 NU7441 Biotechne/Tocris, #3712, **CID:** 11327430
509 DMSO Sigma, D2650, **CID:** 679
510 2'3'-cGAMP InvivoGen, tlrl-nacga23-02, **CID:** 137120248
511 3'3'-cGAMP InvivoGen, tlrl-nacga, **CAS number:** 849214-04-6
512 c-di-AMP InvivoGen, tlrl-nacda, **CAS number:** 2734909-87-4 / 54447-84-6 (free acid)
513 c-di-GMP InvivoGen, tlrl-nacdg, **CAS number:** 2222132-40-1 / 61093-23-0 (free acid).
514 diABZI InvivoGen, tlrl-diabzi-2, **CID:** 137701219, **CAS number:** 2138299-34-8
515 E7766 MedChemExpress, HY-111999A,
516 ADUS100 ammonium salt MedChemExpress, HY-12885B
517 Fluorinated 3'3'-cGAMP Invivogen, tlrl-nacgaf-05, **CAS number**: not available

518 Viral particle production and generation of knock-out cell lines

519 To generate the T98G$^{IFNAR-/-}$ knock-out and control cell lines, lentiviral particles were produced
520 by co-transfection of 2×10^6 293T cells with 5 µg of LentiCRISPRv2GFP plasmid (Addgene #
521 82416) expressing the gRNA targeting the gene of interest or non-targeting control (CTRL)
522 gRNA, 5 µg of psPAX2 and 1 µg of pMD2.G, using the standard calcium phosphate transfection
523 protocol.

524 T98G cells were transduced with lentiviral particles and 72 hours post-transduction GFP-
525 positive cells were sorted and pooled in a 6-well plate using a BD FACS melody. Cells were
526 next amplified and IFNAR levels controlled by WB.

527 HEK293T$^{DNA\text{-}PKcs\text{-}/\text{-}}$ clones and HEK293T^{CTRL} cells were generated by JetPrime (Polyplus)
528 mediated transfection of LentiCRISPRv2GFP plasmid expressing the gRNA targeting the gene
529 of interest or non-targeting control (CTRL) gRNA. Two days later GFP^{+} single-cell clones were
530 selected on a BD FACSAria. Absence of DNA-PK expression was verified by WB.

531 Primers for gRNA expressing constructs:

532 CTRL:
533 CACCGAGCACGTAATGTCCGTGGAT, AAACATCCACGGACATTACGTGCTC
534 IFNAR:
535 CACCGAGCTGACACTCACCTTCCCC, AAACGGGGAAGGTGAGTGTCAGCTC
536 PRKDC:
537 CACCGGCAGGAGACCTTGTCCGCTG, AAACCAGCGGACAAGGTCTCCTGCC

538 Cloning of DNA-PK expression vector:

539 pcDNA3.1-nFlag-DNA-PK was cloned from synthesized gene fragments (eBlocks, IDT) based
540 on consensus sequence ENST00000314191.7 modified for codon optimization. The gRNA
541 binding site targeted for knock-out was modified to prevent targeting by CRISPR/Cas9
542 constructs. N-terminal 3XFlag sequence including $(GGGGS)_3$ linker was added to the
543 synthesized template. pcDNA3.1 backbone was digested using BamHI and EcoRI,
544 dephosphorylated using Quick CIP (NEB) and purified on agarose gel. eBlocks were amplified
545 with KAPA HIFI HotStart Ready Mix (Roche) and purified on agarose gel. Gibson cloning was
546 performed in two steps, with amplified and purified intermediate constructs, using NEBuilder
547 HiFi DNA Assembly Master Mix and NEB Stable Competent *E. coli* grown at 30°C. Resulting
548 plasmid preparations were verified by whole plasmid sequencing.

549 Gene silencing

550 Silencing of DNA-PKcs was achieved in T98G cells using siRNAs and INTERFERin
551 (Polyplus) following the manufacturer's instructions. siRNAs (Dharmacon™; Horizon
552 Discovery) were used:
553 siCTRL: CGUACGCGGAAUACUUCGAUU
554 siDNA-PKcs: GAUCGCACCUUACUCUGUUUU
555 siKU70: ACAAGCAGUGGACCUGACUU

556 Cell treatment and transfection

557 Cells were plated in 6-well plate, or 100 mm dishes. Eighteen hours later, cells were pretreated
558 with 2 μM NU7441 (#3712, Biotechne/Tocris) for 1 hour in DMEM or RPMI, prior to
559 transfection with 2′3′-cGAMP (10 μg/ml, InvivoGen) using Lipofectamine 2000 (Thermo
560 Fischer Scientific), following the manufacturer's instructions. One, three or six hours after
561 transfection, cells were harvested and stored at −80°C prior to 2’3’-cGAMP, protein or RNA
562 extraction.

563 For other drug treatment, following 1 hour preincubation with Nu7441, cells were treated with
564 2’3’-GAM(PS)2 (Rp/Sp) (InvivoGen), or fluorinated 3’3’-cGAMP (InvivoGen) at 10 μg/ml,
565 with diABZI compound 3 (InvivoGen) at 10 μM, with E7766 (MedChemExpress) at 1 μM, or
566 ADUS100 (MedChemExpress) at 50μM. Six hours later, cells were harvested and stored at
567 −80°C prior to protein or RNA extraction.

568 RNA extraction and gene expression analyses

569 Total RNA was isolated with TRIzol (Invitrogen). RNA concentration was measured with a
570 Nanodrop spectrophotometer (ND-1000, Nanodrop Technologies), prior to treatment with
571 TURBO DNase (Ambion) and cDNA synthesis from 1-2 μg RNA using SuperScript IV
572 (Invitrogen) using Oligo(dT) and quantification with a LightCycler 480 cycler (Roche) using
573 SYBR Green Master Mix (Takara) and appropriate primers. Relative quantities of the transcript
574 were calculated using the ΔΔCt method, using the Glyceraldehyde3-phosphate dehydrogenase
575 (*GAPDH*) for normalization, except for THP1 analyses were a normalization with
576 Hypoxanthine Phosphoribosyltransferase 1 (*HPRT1*) and Actin Beta (*ACTB*) was performed.
577 The RT-qPCR primers used are listed below:

578 GAPDH: For: CTGGCGTCTTCACCACCATGG, Rev: CATCACGCCACAGTTTCCCGG
579 ACTB: For: GGACTTCGAGCAAGAGATGG, Rev: AGCACTGTGTTGGCGTACAG
580 HPRT1: For: TGACACTGGCAAAACAATGCA, Rev: GGTCCTTTTCACCAGCAAGCT
581 IFNB1: For: GAATGGGAGGCTTGAATACTGCCT, Rev: TAGCAAAGATGTTCTGGA
582 GCATCTC
583 ISG15:For: GATCACCCAGAAGATCGGCG, Rev: GTTCGTCGCATTTGTCCACC
584 CXCL10: For: GAAAGCAGTTAGCAAGGAAAGGTG, Rev: ATGTAGGGAAGTGATG
585 GGAGAGG
586 IFIT1: For: GCCTTGCTGAAGTGTGGAGGAA, Rev: ATCCAGGCGATAGGCAGAGATC
587 IFIT2: For: GGAGCAGATTCTGAGGCTTTGC, Rev: GGATGAGGCTTCCAGACTCCAA

588 CCL5: For: CCTGCTGCTTTGCCTACATTGC, Rev: ACACACTTGGCGGTTCTTTCGG

589 Whole-cell lysate preparation and Western Blot

590 Cells were lysed in 5 packed cell volumes of TENTG-150 (20 mM Tris–HCl [pH 7.4], 0.5 mM
591 EDTA, 150 mM NaCl, 10 mM KCl, 0.5% Triton X-100, 1.5 mM MgCl2, and 10% glycerol,
592 supplemented with 10 mM β-mercaptoethanol, 0.5 mM PMSF and phosphatase inhibitor
593 (Sigma)) for 30 min at 4°C. Lysates were centrifuged 30 min at 14,000 g, and supernatants
594 were collected for WB. Protein quantification was performed using Bradford assay (Bio-Rad).

595 Protein samples were prepared in Laemmli buffer and heated at 95°C for 5 min prior to
596 resolution by sodium dodecyl sulfate–polyacrylamide gel electrophoresis (SDS-PAGE) using
597 4–15% Mini-PROTEAN® TGX™ Precast Protein Gels (Bio-Rad). Proteins were transferred
598 onto nitrocellulose membranes (Biorad Trans blot turbo). Proteins were visualized on
599 membranes using Ponceau S solution (Sigma-Aldrich) prior to 30 min blocking with (PBS)
600 containing 0.1% Tween (PBS-T) supplemented with 5% milk. Membranes were subsequently
601 incubated with primary antibodies in 5% milk/PBS-T (1:1,000 dilution, except when indicated)
602 for 2 hours at RT. Primary antibodies used include: anti-DNA-PKcs (A300-517, Bethyl, 1:500),
603 anti-cGAS (15102) Cell Signaling Technology), anti-pSTING Ser366 (19781, Cell Signaling
604 Technology), anti-STING (13647, Cell Signaling Technology), anti-pIRF3 Ser386 (ab76493,
605 Abcam), anti-IRF3 (11904, Cell Signaling Technology), anti-HSP90 (4877, Cell Signaling
606 Technology), anti-GAPDH (60004-1-Ig, Proteintech Europe, 1:5,000), αTUBULIN (66031-1-
607 Ig, Proteintech Europe, 1:10,000). Membranes were incubated with Horseradish peroxidase
608 (HRP)-coupled secondary antibodies (Cell Signaling Technology) at 1:2,000 dilution, for 1
609 hour at RT. Immunoreactivity was detected by Chemiluminescence (SuperSignal West Pico or
610 Femto, Thermo Fisher Scientific). Images were acquired on a ChemiDoc (Bio-Rad) or
611 Amersham Imager 680 (GE Healthcare).

612 Endogenous DNA-PKcs and FLAG-DNA-PKcs immunoprecipitation and assessment of
613 interaction with 2'3'-cGAMP interaction

614 For immunoprecipitation of endogenous DNA-PKcs, T98G cells were lysed in 5 packed cell
615 volume of the lysis buffer 20 mM Tris–HCl [pH 7.4], 150 mM NaCl, 10 mM KCl, 0.5% Triton
616 X-100, 1.5 mM MgCl2, and 10% glycerol, supplemented with 10 mM β-mercaptoethanol,
617 0.5 mM PMSF, for 30 min at 4°C on a wheel. Lysates were centrifuged 30 min at 14,000 g,
618 and supernatants were collected for immunoprecipitation. Endogenous immunoprecipitation

619 was performed using DNA-PKcs-targeting antibody (A300-517A, Bethyl), or Rabbit IgG
620 (Santa Cruz) as a negative control. After an overnight incubation at 4°C on a wheel,
621 immunoprecipitation was performed using Protein G Sepharose Fast Flow beads (Sigma). After
622 3 washes in lyses buffer, part of the bound material was either eluted in Laemmli buffer for WB
623 analyses, or used to assess DNA-PKcs:2'3'-cGAMP interaction.

624 FLAG-DNA-PKcs immunoprecipitation was performed by expressing FLAG-DNA-PKcs in
625 293T$^{DNA\text{-}PKcs\text{-}/\text{-}}$ (C#2) for 48 hours prior to whole cell extract preparation as above and
626 immunoprecipitation using anti-FLAG dynabeads. Immunoprecipitates were analyzed by WB
627 or used to assess DNA-PKcs:2'3'-cGAMP interaction

628 To assess DNA-PKcs:2'3'-cGAMP interaction, bound material was incubated with an excess
629 of 2'3'-cGAMP diluted in lyses buffer, for 30 min on ice. After 3 washes with lyses buffer,
630 bound material was subjected to proteinase K treatment (15 min at room temperature) to
631 denature DNA-PKcs and allow the release of potential bound 2'3'-cGAMP. Proteinase K were
632 inactivated, incubating samples 10 min at 95°C, prior to measurement of 2'3'-cGAMP level by
633 enzyme-linked immunosorbent assay (ELISA).

634 <u>Immunoprecipitation of Recombinant DNA-PKcs and assessment of interaction with CDN</u>

635 For the immunoprecipitation of recombinant DNA-PKcs, 2 µg of anti-DNA-PKcs antibody or
636 the corresponding IgG control was incubated with 70 ng of recombinant DNA-PKcs protein
637 (Promega) in 500 µL of lysis buffer (20 mM Tris–HCl [pH 7.4], 150 mM NaCl, 10 mM KCl,
638 0.5% Triton X-100, 1.5 mM MgCl2, and 10% glycerol, supplemented with 10 mM β-
639 mercaptoethanol, 0.5 mM PMSF). The mixture was incubated overnight at 4°C on a rotating
640 wheel. The next day, the samples were centrifuged at 12,000 rpm for 10 min, and the
641 supernatant was collected. Thirty µL of Sepharose beads (5 µL per immunoprecipitation point,
642 for a total of 6 points) were added to the supernatant and incubated at 4°C for 45 min on a
643 rotating wheel. Following incubation, the beads were centrifuged at 2,500 rpm and washed
644 three times with the lysis buffer (without β-mercaptoethanol and PMSF). After washing, the
645 immunoprecipitated complexes were incubated with the tested cyclic dinucleotides (CDNs),
646 including 2'3'-cGAMP, 3'3'-cGAMP, and c-di-AMP, with or without NU7441. The incubation
647 was performed with a CDN or nu7441 concentration 10 times higher than that of DNA-PKcs
648 for 30 min on ice. After the incubation, the beads were washed, and the samples were digested
649 with proteinase K before measuring the amount of CDNs bound to DNA-PKcs by ELISA. 2'3'-

650 cGAMP, 3’3’-cGAMP and c-di-AMP ELISA were performed according to the manufacturer's
651 protocol using the Cayman Chemical 2′3′-cGAMP ELISA Kit (CAY501700), 3′3′-cGAMP
652 ELISA Kit (CAY502130), c-di-AMP ELISA Kit (CAY501960), respectively.

653 Quantificaiton of 2’3’cGAMP in T98G and 293T cells

654 For intracellular 2’3’-cGAMP quantification, T98G or 293T cells were harvested 1 or 3 hours
655 post 2’3’-cGAMP transfection, respectively, counted, washed in phosphate-buffered saline
656 (PBS) (Sigma), pelleted, and either directly processed or frozen at −80°C until extraction. 2’3’-
657 cGAMP extraction was performed using the commercially available Mammalian Protein
658 Extraction Reagent (M-PER) buffer (Thermo Fisher), accordingly to the manufacture protocol.
659 The recovered supernatants were used for 2’3’-cGAMP measurement, following adequate
660 sample dilution. 2’3’-cGAMP amount in each sample was further normalized to the µg of
661 proteins per sample.

662 ATP hydrolysis assay

663 The ability of DNA-PK to hydrolyze ATP was measured by using the DNA-PK Kinase Enzyme
664 System coupled to the ADP-Glo Assay (Promega), following manufacturer’s instructions.
665 Briefly, 30 unit of human recombinant DNA-PK were incubated for 60 min at room temperature
666 with 1 µM ATP, 1 x activator and 0.2 µg/µl substrate, in presence of increasing doses of 2’3’-
667 cGAMP (InvivoGen), 3’3’-cGAMP (InvivoGen), c-di-GMP (InvivoGen), c-di-AMP
668 (InvivoGen), ADUS-100 (MedChemExpress), or E7766 (MedChemExpress). Incubation with
669 4 µM NU7441 was included as a positive control. After 1 hour, the reactions were incubated
670 with 25 µL of ADP-Glo reagent for 40 min at room temperature, followed by incubation with
671 50 µL of Kinase Detection reagent for 30 min at room temperature. Luminescence was
672 measured using the FLUOstar Omega microplate reader (BMG Labtech).

673 Molecular Modelling Analyses

674 3D coordinates were obtained from the X-ray solved, Crystal Structure of Human DNA-
675 dependent Protein Kinase Catalytic Subunit (DNA-PKcs) with RCSB code: 5LUQ. The full
676 amino acid sequence for ATM, ATR and mouse DNA-PK were obtained from GenBank
677 database. The sequence alignment was done using ClustalW. The alignment was repeated using
678 Hidden Markov Models yielding similar results as obtained by ClustalW, due to the
679 conservation of several anchoring motifs throughout the alignment. Molecular docking studies

were executed using the ZDOCK suite, which relies on a three-dimensional fast Fourier transformation algorithm. ZDOCK uses a scoring function that returns electrostatic, hydrophobic and desolvation energies, and performs a fast pairwise-shape complementarity evaluation. Moreover, it uses the contact propensities of transient complexes to perform an evaluation of a pairwise atomic statistical potential for the docking molecular system.

RDOCK was utilized to refine and evaluate the results obtained by ZDOCK. RDOCK performs a fast energy minimization step to the ZDOCK molecular complex outputs and ranks them according to their re-calculated binding free energies. Energy minimizations were used to remove any residual geometrical strain in each molecular system, using the Amber99 force field as it is implemented into the Gromacs suite, version 4.5.5. All Gromacs-related simulations were performed through our previously developed graphical interface. An implicit Generalized Born (GB) solvation was chosen at this stage, to accelerate the energy minimization process. Subsequently, molecular systems were subjected to unrestrained Molecular Dynamics Simulations (MDS) using the Gromacs suite, version 4.5.5. MDS took place in a simple point charge (SPC) water-solvated, periodic environment. Water molecules were added using the truncated octahedron box extending 7Å from each atom. Molecular systems were neutralized with counter-ions as required. For the purposes of this study all MDS were performed using the NVT ensemble (i. e. constant Number of atoms, Volume and Temperature throughout the simulation) in a canonical environment, at 300 K and a step-size equal to 2 femto-seconds for a total 10 nanoseconds simulation time. .

The quality and reliability of produced models in terms of 3D structural conformation was evaluated using the Gromacs package using a residue packing quality function, which depends on the number of buried non-polar side chain groups and on hydrogen bonding and the PROCHECK suite. Finally, the Molecular Operating Environment (MOE) suite was used to evaluate the 3D geometry of the models in terms of their Ramachandran plots, omega torsion profiles, phi/psi angles, planarity, C-beta torsion angles and rotamer strain energy profiles.

<u>HSV-1 Infection</u>

HSV-1-GFP and VSV-GFP infections, quantifications and imaging

The HSV-1 KOS-64-GFP strain (HSV-1-GFP) was a gift from S. R. Paludan (Aarhus university, Danemark). HSV-1 was amplified on Vero cells, aliquoted and frozen at -80°C.

710 Titration was performed on Vero cells, by serial dilutions and plaque formation assessment to
711 determine the multiplicity of infection (MOI).

712 VSV-GFP was a gift from Dr Sebastien Pfeffer (IBMC, France). VSV-GFP was amplified on
713 BHK21 cells, aliquoted and frozen at -80°C. Single-round titration of the viral stock was
714 performed on NIH-3T3 cells to determine the MOI.

715 2x104 T98G cells were seeded in 96 well plates in technical triplicates. The next morning, cells
716 were pretreated or not for 1h with 2µM of NU7441. Cells were subsequently treated for 6h with
717 either 10µM of diABZi, 1µM of E7766 or 10µg/ml of fluorinated 3'3'-cGAMP in the presence
718 or not of 2µM NU7441. The cells were then infected with either HSV-1-GFP (for 1.5 h at MOI
719 2) or VSV-GFP (for 1 h at MOI 0.1) in DMEM without serum. Media was then replaced with
720 either DMEM-10% FBS (VSV-GFP) or DMEM-1% human serum overnight and replaced with
721 DMEM-10% FBS the next morning (HSV-1-GFP). Cells were fixed with 4% PFA for 20 min
722 either 16 h post-infection (for VSV-GFP) or 48 h post-infection (for HSV-1-GFP). Cells were
723 permeabilized with 0.2% Triton X-100 for 10 minutes at room temperature and nuclei were
724 stained with DAPI.

725 The percentage of infected cells (i.e. GFP-positive cells) was quantified using an ImageXpress
726 Pico (Molecular Devices) with a 4X lens. Values were averaged between technical triplicates.

727 Statistical analysis

728 Statistical analysis was performed using GraphPad Prism software. To compare data from two
729 conditions, a standard unpaired two-tailed Student's t test was performed. One-way Anova with
730 Tukey's multiple comparisons test was used to analyze the ATP hydrolyses assay. The number
731 of replicates in each experiment are indicated in the figure legends. All data are expressed as
732 mean ± SEM. Results were considered significant when $p < 0.05$. Ns: non-significant.
733 *P < 0.05, **P < 0.01, ***P < 0.001 and ****P < 0.0001

734

735 **References**

736 1 Crowl, J. T., Gray, E. E., Pestal, K., Volkman, H. E. & Stetson, D. B. Intracellular Nucleic Acid
737 Detection in Autoimmunity. *Annu Rev Immunol* **35**, 313-336, doi:10.1146/annurev-immunol-
738 051116-052331 (2017).
739 2 Motwani, M., Pesiridis, S. & Fitzgerald, K. A. DNA sensing by the cGAS-STING pathway in
740 health and disease. *Nat Rev Genet* **20**, 657-674, doi:10.1038/s41576-019-0151-1 (2019).
741 3 Ablasser, A. & Chen, Z. J. cGAS in action: Expanding roles in immunity and inflammation.
742 *Science* **363**, doi:10.1126/science.aat8657 (2019).
743 4 Sun, Z. & Hornung, V. cGAS-STING signaling. *Curr Biol* **32**, R730-R734,
744 doi:10.1016/j.cub.2022.05.027 (2022).

5 Ou, L., Zhang, A., Cheng, Y. & Chen, Y. The cGAS-STING Pathway: A Promising Immunotherapy Target. *Front Immunol* **12**, 795048, doi:10.3389/fimmu.2021.795048 (2021).
6 Decout, A., Katz, J. D., Venkatraman, S. & Ablasser, A. The cGAS-STING pathway as a therapeutic target in inflammatory diseases. *Nat Rev Immunol* **21**, 548-569, doi:10.1038/s41577-021-00524-z (2021).
7 Sun, L., Wu, J., Du, F., Chen, X. & Chen, Z. J. Cyclic GMP-AMP synthase is a cytosolic DNA sensor that activates the type I interferon pathway. *Science* **339**, 786-791, doi:10.1126/science.1232458 (2013).
8 Wu, J. *et al.* Cyclic GMP-AMP is an endogenous second messenger in innate immune signaling by cytosolic DNA. *Science* **339**, 826-830, doi:10.1126/science.1229963 (2013).
9 Sun, W. *et al.* ERIS, an endoplasmic reticulum IFN stimulator, activates innate immune signaling through dimerization. *Proc Natl Acad Sci U S A* **106**, 8653-8658, doi:10.1073/pnas.0900850106 (2009).
10 Zhong, B. *et al.* The adaptor protein MITA links virus-sensing receptors to IRF3 transcription factor activation. *Immunity* **29**, 538-550, doi:10.1016/j.immuni.2008.09.003 (2008).
11 Hertzog, J. & Rehwinkel, J. Regulation and inhibition of the DNA sensor cGAS. *EMBO Rep* **21**, e51345, doi:10.15252/embr.202051345 (2020).
12 Vila, I. K., Guha, S., Kalucka, J., Olagnier, D. & Laguette, N. Alternative pathways driven by STING: From innate immunity to lipid metabolism. *Cytokine Growth Factor Rev* **68**, 54-68, doi:10.1016/j.cytogfr.2022.08.006 (2022).
13 Hou, Y. *et al.* SMPDL3A is a cGAMP-degrading enzyme induced by LXR-mediated lipid metabolism to restrict cGAS-STING DNA sensing. *Immunity* **56**, 2492-2507 e2410, doi:10.1016/j.immuni.2023.10.001 (2023).
14 Li, L. *et al.* Hydrolysis of 2'3'-cGAMP by ENPP1 and design of nonhydrolyzable analogs. *Nat Chem Biol* **10**, 1043-1048, doi:10.1038/nchembio.1661 (2014).
15 Mardjuki, R. *et al.* Identification of extracellular membrane protein ENPP3 as a major cGAMP hydrolase, cementing cGAMP's role as an immunotransmitter. *bioRxiv*, doi:10.1101/2024.01.12.575449 (2024).
16 Jutte, B. B. *et al.* Intercellular cGAMP transmission induces innate immune activation and tissue inflammation in Trex1 deficiency. *iScience* **24**, 102833, doi:10.1016/j.isci.2021.102833 (2021).
17 McWhirter, S. M. *et al.* A host type I interferon response is induced by cytosolic sensing of the bacterial second messenger cyclic-di-GMP. *J Exp Med* **206**, 1899-1911, doi:10.1084/jem.20082874 (2009).
18 Woodward, J. J., Iavarone, A. T. & Portnoy, D. A. c-di-AMP secreted by intracellular Listeria monocytogenes activates a host type I interferon response. *Science* **328**, 1703-1705, doi:10.1126/science.1189801 (2010).
19 Burleigh, K. *et al.* Human DNA-PK activates a STING-independent DNA sensing pathway. *Sci Immunol* **5**, doi:10.1126/sciimmunol.aba4219 (2020).
20 Ferguson, B. J., Mansur, D. S., Peters, N. E., Ren, H. & Smith, G. L. DNA-PK is a DNA sensor for IRF-3-dependent innate immunity. *Elife* **1**, e00047, doi:10.7554/eLife.00047 (2012).
21 Hristova, D. B. *et al.* DNA-PKcs is required for cGAS/STING-dependent viral DNA sensing in human cells. *iScience* **27**, 108760, doi:10.1016/j.isci.2023.108760 (2024).
22 Taffoni, C. *et al.* DNA damage repair kinase DNA-PK and cGAS synergize to induce cancer-related inflammation in glioblastoma. *EMBO J* **42**, e111961, doi:10.15252/embj.2022111961 (2023).
23 Sun, X. *et al.* DNA-PK deficiency potentiates cGAS-mediated antiviral innate immunity. *Nat Commun* **11**, 6182, doi:10.1038/s41467-020-19941-0 (2020).
24 Leahy, J. J. *et al.* Identification of a highly potent and selective DNA-dependent protein kinase (DNA-PK) inhibitor (NU7441) by screening of chromenone libraries. *Bioorg Med Chem Lett* **14**, 6083-6087, doi:10.1016/j.bmcl.2004.09.060 (2004).
25 Paulis, A. & Tramontano, E. Unlocking STING as a Therapeutic Antiviral Strategy. *Int J Mol Sci* **24**, doi:10.3390/ijms24087448 (2023).
26 Yue, X., Bai, C., Xie, D., Ma, T. & Zhou, P. K. DNA-PKcs: A Multi-Faceted Player in DNA Damage Response. *Front Genet* **11**, 607428, doi:10.3389/fgene.2020.607428 (2020).

27 Zhang, X. *et al.* Cyclic GMP-AMP containing mixed phosphodiester linkages is an endogenous high-affinity ligand for STING. *Mol Cell* **51**, 226-235, doi:10.1016/j.molcel.2013.05.022 (2013).
28 Burdette, D. L. *et al.* STING is a direct innate immune sensor of cyclic di-GMP. *Nature* **478**, 515-518, doi:10.1038/nature10429 (2011).
29 Jin, L. *et al.* MPYS is required for IFN response factor 3 activation and type I IFN production in the response of cultured phagocytes to bacterial second messengers cyclic-di-AMP and cyclic-di-GMP. *J Immunol* **187**, 2595-2601, doi:10.4049/jimmunol.1100088 (2011).
30 Perry, A. K., Chen, G., Zheng, D., Tang, H. & Cheng, G. The host type I interferon response to viral and bacterial infections. *Cell Res* **15**, 407-422, doi:10.1038/sj.cr.7290309 (2005).
31 Lees-Miller, J. P. *et al.* Uncovering DNA-PKcs ancient phylogeny, unique sequence motifs and insights for human disease. *Prog Biophys Mol Biol* **163**, 87-108, doi:10.1016/j.pbiomolbio.2020.09.010 (2021).
32 Meek, K., Dang, V. & Lees-Miller, S. P. DNA-PK: the means to justify the ends? *Adv Immunol* **99**, 33-58, doi:10.1016/S0065-2776(08)00602-0 (2008).
33 Blackford, A. N. & Jackson, S. P. ATM, ATR, and DNA-PK: The Trinity at the Heart of the DNA Damage Response. *Mol Cell* **66**, 801-817, doi:10.1016/j.molcel.2017.05.015 (2017).
34 Harding, S. M. *et al.* Mitotic progression following DNA damage enables pattern recognition within micronuclei. *Nature* **548**, 466-470, doi:10.1038/nature23470 (2017).
35 Taffoni, C. *et al.* Nucleic Acid Immunity and DNA Damage Response: New Friends and Old Foes. *Front Immunol* **12**, 660560, doi:10.3389/fimmu.2021.660560 (2021).
36 Wu, J. *et al.* The multifaceted functions of DNA-PKcs: implications for the therapy of human diseases. *MedComm (2020)* **5**, e613, doi:10.1002/mco2.613 (2024).
37 Hines, J. B., Kacew, A. J. & Sweis, R. F. The Development of STING Agonists and Emerging Results as a Cancer Immunotherapy. *Curr Oncol Rep* **25**, 189-199, doi:10.1007/s11912-023-01361-0 (2023).
38 Yang, H., Yao, F., Marti, T. M., Schmid, R. A. & Peng, R. W. Beyond DNA Repair: DNA-PKcs in Tumor Metastasis, Metabolism and Immunity. *Cancers (Basel)* **12**, doi:10.3390/cancers12113389 (2020).